Combust. Theory Modelling **3** (1999) 103–122. Printed in the UK PII: S1364-7830(99)94093-7

Thermal explosion theory for shear localizing energetic solids

Joseph M Powers†

Department of Aerospace and Mechanical Engineering, University of Notre Dame, Notre Dame, IN 46556-5637, USA

Received 8 May 1998, in final form 28 October 1998

Abstract. The behaviour of energetic solids subjected to simple shear loading is modelled to predict ignition. The model is transient, one dimensional and includes effects of thermal diffusion, plastic work and exothermic reaction with one-step irreversible Arrhenius kinetics. A common power-law constitutive model for shear stress which accounts for strain hardening, strain-rate hardening and thermal softening is used. For the energetic solid composite LX-14 subjected to an average strain rate of $\overline{\dot{\gamma}} = 2800\ \mathrm{s}^{-1}$, the model predicts reactive shear localization after an induction time of approximately $t = 5$ ms, in which regions of high strain rate ($\dot{\gamma} > 20\,000\ \mathrm{s}^{-1}$) are confined to thin spatial zones. An approximate thermal explosion theory which enforces spatially homogeneous stress, temperature and reaction progress as well as accounting for the early-time dominance of plastic work over exothermic reaction allows the development of simple analytic expressions for the temporal evolution of all variables. The simple expressions give predictions which agree well with both: (a) numerical predictions of a spatially homogeneous theory which allows simultaneous influences of reaction and plastic work and (b) numerical predictions of a spatially inhomogeneous theory which accounts for spatial stress distributions, thermal diffusion and spatially localized reaction. In particular, the induction time to ignition is captured accurately by the approximate theory; hence, while reactive shear localization may accompany an ignition event, ignition causality is most dependent on plastic work done during the time of spatially homogeneous shear.

1. Introduction

A full understanding of detailed ignition mechanisms in energetic solids subjected to mechanical loading does not currently exist. Under commonly encountered strong-shock loading conditions, energetic solids are stressed well beyond their yield stress, and are often modelled by equations of state similar to those used for fluids. However, a stress model which accounts for the influences of strain, strain rate and temperature is more appropriate for an energetic solid subjected to a milder dynamic mechanical loading event which is still of sufficient strength to induce an ignition event on a longer time scale. Such a loading event may be likely to occur in a variety of accident scenarios. As the key to ignition is thought to be the formation of spatially localized hot spots [1], factors which influence the dissipation rate and localization of an input of mechanical energy into thermal energy are thought to be critical. The dissipation rate and localization behaviour are strong functions of material properties of the energetic material.

While many mechanisms have been proposed for hot spot formation (e.g. jetting, void collapse, viscous heating, shock interaction or friction, cf [2]), attention is focused here on one commonly discussed mechanism: shear localization, also known as shear banding. Shear

† E-mail address: powers@nd.edu

1364-7830/99/010103+20$19.50

localization has been widely studied in inert materials, e.g. [3, 4]; additionally, experimental evidence of shear localization in both homogeneous and heterogeneous energetic solids, e.g. [5, 6], and reactive metallic powders [7] has been reported. Other relevant studies include [8–20]. Chaudhri [21] argues that shear, whether localized or not, can only serve as an ignition mechanism when strains are high, and that it remains to be seen whether brittle explosive crystals can sustain sufficiently high strain. He concludes [22] that friction is a more likely cause. While brittle fracture is likely to inhibit shear localization, there is evidence in other materials that increasing hydrostatic stress, such as may be likely in a detonation, can serve to suppress this failure mechanism [23]. Moreover, Frey [24] argues that on a microscopic level, ordinary sliding friction and shear localization are actually identical processes, as frictional forces are due to plastic work done during asperity contact.

Shear localization is thought to evolve in the following manner. A material which exhibits strain hardening, strain-rate hardening and thermal softening is put in a state of spatially uniform shear strain. As the material strains, strain hardening will increase the stress, while thermal softening, which arises due to plastic work, tends to decrease stress. If the material has a local heterogeneity of sufficient magnitude, a locally higher strain rate can be induced. While this gives rise to strain-rate hardening, it also induces more thermal softening. Often, thermal diffusion is too slow a process to remove accumulated thermal energy and the process can accelerate and lead to dominance of thermal softening and ultimate material failure. As temperatures in the zone of shear localization are often sufficiently high to induce chemical reaction, their consideration as an ignition mechanism is natural.

There are few models which consider shear localization accompanied by chemical reaction. The most relevant studies are those of Frey [24], Dienes [25], Caspar [26] and Caspar *et al* [27]. Frey models 2, 4, 6-trinitrotoluene (TNT) as a reactive linearly viscoplastic material in which the coefficient of viscosity has a temperature dependence. Strain dependence is not included in his constitutive model, nor is his model calibrated to experiments under high strain-rate conditions. In some calculations a melt layer is included. The shear band is initiated by assuming that a thin region exists which already has localized shear. In regions of shear localization, velocities, pressures and temperatures of around 0.2 km s^{-1}, 1 GPa and 2000 K, respectively, are predicted. A temperature rise to 1100 K is attributed to plastic heating during the first 35 ns of calculation, at which time reaction over about 25 ns commences, causing a further increase in temperature, which is continuing to rise at cessation of the calculation. Numerical values of pressure and velocity are approaching those of a detonation. Dienes finds time-independent solutions for the spatial structure of temperature, considering a slab with isothermal boundaries subjected to exothermic reaction and uniform plastic heating. He predicts critical slab thicknesses which induce high-temperature reaction in cyclotetramethylene-tetranitramine (HMX) at shear stresses and strain rates up to $\tau = 100$ MPa and $\dot{\gamma} = 10^4$ s^{-1}, respectively. Predictions of shear band formation are not possible as the time dependence, influence of temperature, strain and strain rate on stress and momentum are not included in his model.

Caspar and Caspar *et al* study behaviour of the commonly used heterogeneous solid explosive LX-14 undergoing shear loading. Data taken at high average strain rate, $\overline{\dot{\gamma}} = 300$ and 2800 s^{-1} (where the overbar indicates a spatial average), for an inert simulant of LX-14, Mock 900-20, from a torsional split Hopkinson bar are used to calibrate a constitutive model for stress in terms of strain and strain rate. As described in detail in [27], the simulant is used for safety purposes and contains barium nitrate and pentek crystals of similar density and size distribution as that of reactive HMX particles in a nearly identical binder to that used in LX-14. The constitutive model is then employed in a general one-dimensional unsteady model to predict the thermomechanical response to an input of mechanical energy. Ignition is shown to

be relatively sensitive to changes in mechanical properties, specific heat and activation energy, and relatively insensitive to variation in heat release, thermal conductivity and kinetic rate constant. The study extends that of both Frey and Dienes by including a constitutive model verified under high strain-rate conditions. Further, it is not presupposed that localization has commenced; instead localization is allowed to develop from a small perturbation. Also a detailed account of the development of spatio-temporal fields of velocity, displacement, stress, temperature and reaction progress, along with a sensitivity study is reported. Lastly, relative to Frey, much lower magnitudes of stress and strain rate are studied, such as might be more common in an accident scenario rather than an already established detonation; thus, a direct comparison of results is difficult.

The present study extends the work of [26, 27] by developing a thermal explosion theory which accurately describes the onset of a spatially homogeneous reaction in a material subjected to spatially uniform shear strain. In contrast to the time-independent theory of Dienes, the thermal explosion theory developed here has the ability to predict induction times, but is incapable of predicting reactive shear band thicknesses, due to neglect of spatial gradients. When spatial variations are included, the shear band thickness can be estimated; however, the continual input of plastic work prevents the shear band thickness from reaching a time-independent value.

The remainder of this paper is structured as follows. For completeness, we first present the mathematical model. The model is nearly identical to that of [27], slightly simplified so that a spatial disturbance in initial temperature, rather than geometry, induces localization. At this point, we depart from our earlier work. After recasting the model in dimensionless form, we give limiting assumptions under which a simple analytic description of displacement, velocity, temperature and stress during build-up to reaction is available via an approximate analysis. An algebraic relation is found which predicts the induction time of thermal explosion. Analytic estimates are made for the time scales of vigorous reaction, and an analytic description of the still straining material after reaction is given. In the high activation energy limit and for special choices of material parameters, we find an expression for the induction time through use of a more formal asymptotic analysis. Results of the spatially homogeneous thermal explosion theory are shown to agree well with predictions of the spatially inhomogeneous model. The paper is concluded after determining the sensitivity of the induction time to the magnitude of the initial temperature perturbation. All results are obtained for parameters appropriate for LX-14; however, the theory may be applied to a variety of energetic solids when the necessary constitutive data become available.

2. Mathematical model

The mathematical model is given here. The geometry is that of a thin-walled cylinder (sketched in figure 1). The specimen is loaded at time $t = 0$ such that the origin at axial distance $z = 0$ is stationary, the end $z = L$ is at constant circumferential velocity v_L, and the initial spatial variation of circumferential velocity $v_\theta(z, 0)$, is linear for $z \in [0, L]$. For tractability, the model neglects many features found in real physical systems, for example, detailed chemical kinetics, variable material properties, porosity, material compressibility, glass transition, material melting, latent heat, effects of microstructural heterogeneities, crystal lattice effects and gas phase effects of reaction products. While a general theory may require such ingredients, these are not critical features necessary for a phenomenological description of reactive shear localization.

The following specific assumptions are made. There is no component of velocity or displacement in radial or axial directions. This is reasonable given that the imposed velocity

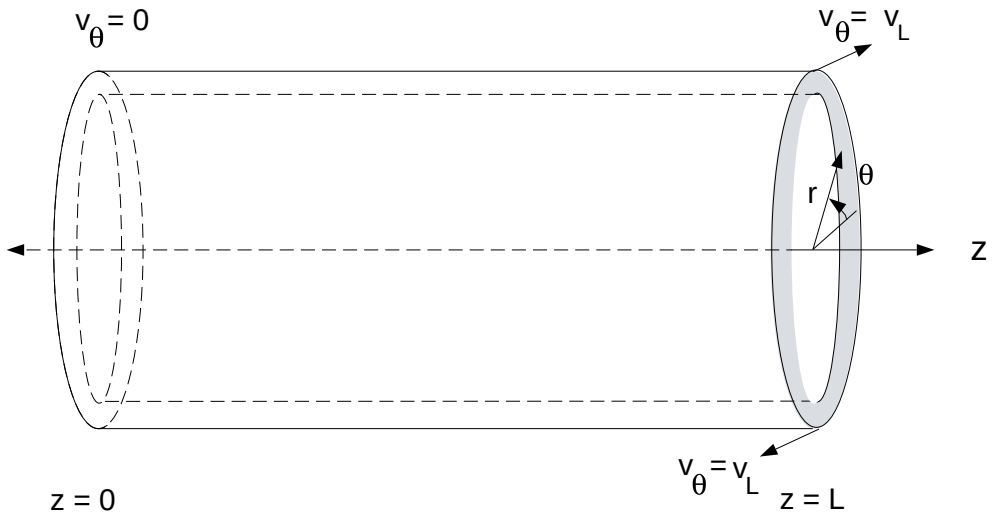

Figure 1. Model geometry.

at $z = L$ is purely circumferential. Due to axisymmetry and the thin-walled geometry, there is negligible variation in circumferential or radial directions. Under these assumptions, the stress tensor reduces to one non-zero component on the axial face in the circumferential direction, which will be referred to as the shear stress. The material is taken to undergo a one-step irreversible exothermic chemical reaction. While progress is being made in formulating detailed kinetic models for energetic solids (see, for example, [28]) it is well known that global one-step models can predict ignition times accurately over many orders of magnitude of time. All material properties are taken to be equal and constant in unreacted and reacted material. We take numerical values for most material and kinetic properties, such as density, thermal conductivity, specific heat, chemical heat release and kinetic rate constants, from a standard source, Dobratz and Crawford [29], using values for the unreacted solid. In actuality, material properties do change on phase transition from solid to gas; however, for many parameters the change is not great. For example the model of Baer and Nunziato [30], which considers granular HMX reacting to form gaseous products, uses a specific heat for the gas which is roughly twice that of the solid. Moreover, upon reaction in a detonation environment, gas phase densities are of a similar order of magnitude to solid phase densities. It is noted that under extreme conditions of fast exothermic reaction that many of these parameters are not known with great accuracy, but are the best available estimates.

As will be seen in the results section, use of these standard assumptions gives rise to temperature predictions ($T \sim 5800$ K) that at first glance may appear to be unreasonably high, especially since these energetic solids are known to melt near 500 K. We note, however, that:

(a) our effectively one-material model can be thought of as modelling reaction products with the same properties as the solid phase; phase change corresponds to a dramatic loss of material strength near the melting temperature; moreover, such high temperatures are not uncommon in gas phase products;
(b) the predictions are entirely consistent with all conservation principles; chemical energy is converted to thermal energy and, on the very fast time scales of chemical reaction, there is insufficient time for diffusion to dampen the temperature peaks; a straightforward extension to a two-material model which accounted for the higher specific heat of product

gases would correspondingly lower the temperature of the products but have a minimal effect on the induction time;

(c) temperature predictions of two-material models for similar materials in detonation conditions are actually near 10 000 K for the gas phase [30]; the higher temperatures can be attributed to additional work done by irreversible shock heating;

(d) though the high temperatures predicted here are mainly due to exothermic reaction, we note that shear band formation in inert materials is also characterized by high temperature; DiLellio and Olmstead [32] report temperatures near 4000 K for steel subjected to a homogeneous strain rate of 1000 s^{-1}.

As many studies, e.g. [30, 31], consider the role of compressibility and acoustic wave propagation in the transition to detonation, we briefly consider here the time scales for which the incompressibility assumption should hold. Incompressibility implies that acoustic processes have had sufficient time to relax. For a specimen of length L with acoustic speed c_A, this implies relaxation after several acoustic time constants $t_A = L/c_A$ have elapsed. For specimen lengths $L \sim 1$ mm and typical acoustic speeds $c_A \sim 10^3$ m s^{-1}, this implies $t_A \sim 1$ μs.

For brevity, we do not give a detailed discussion of how these assumptions can be justified based on an asymptotic analysis of a more general set of equations. It is noted that similar restrictions are commonly adopted in nearly all the current shear banding literature, e.g. [4, 24]. It is plausible that most of the assumptions adopted are appropriate for capturing the essence of a reactive shear band while at the same time minimizing the complexity of the model.

2.1. Dimensional equations

Under these assumptions, the dimensional governing equations are:

$$\rho \frac{\partial v_\theta}{\partial t} = \frac{\partial \tau}{\partial z} \tag{1}$$

$$\rho \frac{\partial e}{\partial t} = \tau \frac{\partial v_\theta}{\partial z} - \frac{\partial q_z}{\partial z} \tag{2}$$

$$\frac{\partial \lambda}{\partial t} = a(1-\lambda) \exp\left(- \frac{E}{\Re T} \right) \tag{3}$$

$$\frac{\partial u_\theta}{\partial t} = v_\theta \tag{4}$$

$$\tau = \alpha \left(\frac{T}{T_0} \right)^{\nu} \left(\frac{\partial u_\theta}{\partial z} \right)^{\eta} \left(\frac{\partial v_\theta}{\partial z} \frac{L}{v_L} \right)^{\mu} \tag{5}$$

$$q_z = -k \frac{\partial T}{\partial z} \tag{6}$$

$$e = cT - \lambda \tilde{q}. \tag{7}$$

There are seven variables, all assumed to be, at most, functions of z and t, in these seven equations: circumferential velocity v_θ, circumferential displacement u_θ, shear stress τ, internal energy per unit mass e, axial heat flux q_z, reaction progress $\lambda \in [0, 1]$ and temperature T. The parameters in equations (1)–(7) are the density ρ, kinetic rate constant a, activation energy E, universal gas constant $\Re$, stress constant α, ambient temperature T_0, thermal softening exponent ν, strain hardening exponent η, strain-rate hardening exponent μ, thermal conductivity k, specific heat c and chemical energy per unit mass $\tilde{q}$. Equation (1) models conservation of linear momentum in the circumferential direction. Equation (2) describes conservation of energy. Equation (3) is a one-step Arrhenius kinetics model. Equation (4) defines velocity. Equations (5)–(7) are constitutive relations for stress, heat flux and internal energy, respectively.

These equations are all commonly used in the general solid mechanics and combustion literature. Equation (5), proposed by Clifton *et al* [33], is an empirically motivated equation and is often employed to model material behaviour under high strain-rate conditions. While equation (5) has the advantage of being able to fit data well, a simple consideration of the second law shows that it is somewhat restricted in validity. Specializing the Gibbs equation for entropy s for an incompressible substance, we obtain $T\,\mathrm{d}s = \mathrm{d}e$. Using this to eliminate e in favour of s in equation (2), substituting for τ and q_z from equations (5) and (6) and separating the heat flux terms into reversible and irreversible parts gives an equation for the evolution of entropy:

$$\rho\frac{\partial s}{\partial t} = \frac{\alpha}{T}\left(\frac{T}{T_0}\right)^{\nu}\left(\frac{\partial u_\theta}{\partial z}\right)^{\eta}\left(\frac{\partial v_\theta}{\partial z}\right)^{\mu+1}\left(\frac{L}{v_L}\right)^{\mu} + \frac{k}{T^2}\left(\frac{\partial T}{\partial z}\right)^2 + k\frac{\partial}{\partial z}\left(\frac{1}{T}\frac{\partial T}{\partial z}\right). \tag{8}$$

With the second law of thermodynamics requiring that

$$\rho\frac{\partial s}{\partial t} \geqslant k\frac{\partial}{\partial z}\left(\frac{1}{T}\frac{\partial T}{\partial z}\right) \tag{9}$$

substitution of equation (8) into equation (9) gives a Clausius–Duhem inequality in weak form:

$$\frac{\alpha}{T}\left(\frac{T}{T_0}\right)^{\nu}\left(\frac{\partial u_\theta}{\partial z}\right)^{\eta}\left(\frac{\partial v_\theta}{\partial z}\right)^{\mu+1}\left(\frac{L}{v_L}\right)^{\mu} + \frac{k}{T^2}\left(\frac{\partial T}{\partial z}\right)^2 \geqslant 0. \tag{10}$$

The two terms in equation (10) describe entropy production due to irreversible plastic work and heat transfer. The strong form of the Clausius–Duhem inequality requires that each individual contribution to irreversibility must also be positive. For the heat transfer component, this requires simply that $k \geqslant 0$. The plastic work component is less general. Sufficient conditions are those present in the experiment from which the model was developed, namely

$$\frac{\partial u_\theta}{\partial z} \geqslant 0 \qquad \frac{\partial v_\theta}{\partial z} \geqslant 0 \tag{11}$$

in addition to $T > 0$, $\alpha \geqslant 0$, $L \geqslant 0$, $v_L > 0$ and $T_0 > 0$. These conditions are maintained in our simulations, so all results presented satisfy the second law of thermodynamics. That said, a more robust constitutive theory without such restrictions, which additionally had full multidimensional tensorial formalism, would be advantageous over the present model.

The following boundary conditions are sufficient to describe the system, which is held fixed at one end, rotated at the other and thermally insulated at both:

$$\begin{aligned} &v_\theta(t,0) = 0 \qquad v_\theta(t,L) = v_L \qquad u_\theta(t,0) = 0 \qquad u_\theta(t,L) = v_L t \\ &\frac{\partial T}{\partial z}(t,0) = 0 \qquad \frac{\partial T}{\partial z}(t,L) = 0. \end{aligned} \tag{12}$$

For initial conditions, at $t = 0^-$ we take the system to be at rest and undisplaced. Then at $t = 0$, we impose a sudden acceleration to a state in which the spatial velocity distribution is linear, while the specimen remains undisplaced. The initial temperature is taken to be uniform, except for a small positive perturbation around $z = \frac{1}{2}L$. The conditions at $t = 0$ are thus

$$\begin{aligned} &v_\theta(0,z) = v_L\frac{z}{L} \qquad u_\theta(0,z) = 0 \qquad \lambda(0,z) = 0 \\ &T(0,z) = \begin{cases} T_0 & z \notin \left[\frac{1}{2}L(1-\hat{\epsilon}_L), \frac{1}{2}L(1+\hat{\epsilon}_L)\right] \\ T_0(1+\hat{\epsilon}_T) & z \in \left[\frac{1}{2}L(1-\hat{\epsilon}_L), \frac{1}{2}L(1+\hat{\epsilon}_L)\right]. \end{cases} \end{aligned} \tag{13}$$

Here $\hat{\epsilon}_L \ll 1$ and $\hat{\epsilon}_T \ll 1$ are small dimensionless parameters which characterize the local width and amplitude, respectively, of the temperature disturbance.

While equations (1)–(13) are sufficient to describe a well-posed initial-boundary value problem, it is also common to discuss results in terms of strain and strain rate and, to that end, the following standard definitions are introduced. We take strain γ to be

$$\gamma = \frac{\partial u_\theta}{\partial z}. \tag{14}$$

With this definition, various representations of strain rate, that is the partial derivative of strain with respect to time, commonly denoted as $\dot{\gamma}$, are available:

$$\dot{\gamma} = \frac{\partial \gamma}{\partial t} = \frac{\partial}{\partial t}\frac{\partial u_\theta}{\partial z} = \frac{\partial}{\partial z}\frac{\partial u_\theta}{\partial t} = \frac{\partial v_\theta}{\partial z}. \tag{15}$$

Lastly, the average strain rate is simply

$$\overline{\dot{\gamma}} = \frac{1}{L}\int_0^L \frac{\partial v_\theta}{\partial z}\,\mathrm{d}z = \frac{v_L}{L}. \tag{16}$$

2.2. Dimensionless equations

The governing equations are reduced as follows. First the constitutive equations (5)–(7) are substituted into equations (1)–(3) so as to eliminate τ, q_z and e. Next, using a star subscript to denote a dimensionless variable, we introduce scaled independent variables

$$z_* = \frac{z}{L} \qquad t_* = \frac{v_L}{L}t \tag{17}$$

and scaled dependent variables

$$v_* = \frac{v_\theta}{v_L} \qquad T_* = \frac{T}{T_0} \qquad \lambda_* = \lambda \qquad u_* = \frac{u_\theta}{L}. \tag{18}$$

With these operations, equations (1)–(4) are restated as a system of four nonlinear partial differential equations in the four unknowns, v_*, T_*, λ_* and u_*:

$$\frac{\partial v_*}{\partial t_*} = \hat{\alpha}\frac{\partial}{\partial z_*}\left(T_*^{\nu}\left(\frac{\partial u_*}{\partial z_*}\right)^{\eta}\left(\frac{\partial v_*}{\partial z_*}\right)^{\mu}\right) \tag{19}$$

$$\frac{\partial T_*}{\partial t_*} = \hat{\alpha}\widehat{Ec}T_*^{\nu}\left(\frac{\partial u_*}{\partial z_*}\right)^{\eta}\left(\frac{\partial v_*}{\partial z_*}\right)^{\mu+1} + \frac{1}{\widehat{Pe}}\frac{\partial^2 T_*}{\partial z_*^2} + \hat{a}\hat{q}(1-\lambda_*)\exp\left(-\frac{\hat{\Theta}}{T_*}\right) \tag{20}$$

$$\frac{\partial \lambda_*}{\partial t_*} = \hat{a}(1-\lambda_*)\exp\left(-\frac{\hat{\Theta}}{T_*}\right) \tag{21}$$

$$\frac{\partial u_*}{\partial t_*} = v_* \tag{22}$$

with boundary and initial conditions

$$v_*(t_*, 0) = 0 \quad v_*(t_*, 1) = 1 \quad u_*(t_*, 0) = 0 \quad u_*(t_*, 1) = t_*$$
$$\frac{\partial T_*}{\partial z_*}(t_*, 0) = 0 \qquad \frac{\partial T_*}{\partial z_*}(t_*, 1) = 0 \quad v_*(0, z_*) = z_* \quad u_*(0, z_*) = 0 \quad \lambda_*(0, z_*) = 0$$
$$T(0, z_*) = \begin{cases} 1 & z_* \notin \left[\frac{1}{2}(1-\hat{\epsilon}_L), \frac{1}{2}(1+\hat{\epsilon}_L)\right] \\ 1+\hat{\epsilon}_T & z_* \in \left[\frac{1}{2}(1-\hat{\epsilon}_L), \frac{1}{2}(1+\hat{\epsilon}_L)\right]. \end{cases} \tag{23}$$

Six new dimensionless parameters, where the hat notation is employed for dimensionless constants, arise in the scaling:

$$\begin{aligned} \hat{\alpha} &= \frac{\alpha}{\rho v_L^2} & \widehat{Ec} &= \frac{v_L^2}{cT_0} & \widehat{Pe} &= \frac{\rho c}{k}v_L L \\ \hat{q} &= \frac{\tilde{q}}{cT_0} & \hat{a} &= \frac{L}{v_L}a & \hat{\Theta} &= \frac{E}{\Re T_0}. \end{aligned} \tag{24}$$

Here $\hat{\alpha}$ is the scaled stress constant, $\widehat{Ec}$ is the Eckert number, $\widehat{Pe}$ is the Peclet number, $\hat{q}$ is the scaled heat release, $\hat{a}$ is the scaled kinetic constant and $\hat{\Theta}$ is the scaled activation energy.

It is also useful to define dimensionless shear stress and heat flux as $\tau_* = \tau/\rho v_L^2$, $q_{z*} = (Lk/T_0)q_z$. With these definitions, constitutive equations for shear stress and heat flux can be written as

$$\tau_* = \hat{\alpha} T_*^{\nu} \left(\frac{\partial u_*}{\partial z_*} \right)^{\eta} \left(\frac{\partial v_*}{\partial z_*} \right)^{\mu} \tag{25}$$

$$q_{z*} = -\frac{\partial T_*}{\partial z_*}. \tag{26}$$

Also, we take $\gamma_* = \gamma$, $\dot{\gamma}_* = \dot{\gamma}(L/v_L)$, so that

$$\frac{\partial u_*}{\partial z_*} = \gamma_* \tag{27}$$

$$\frac{\partial \gamma_*}{\partial t_*} = \dot{\gamma}_* \tag{28}$$

$$\frac{\partial v_*}{\partial z_*} = \dot{\gamma}_*. \tag{29}$$

With the use of the above definitions, necessary to cast the governing equations as a system of first-order partial differential equations, it is easily shown using the methods outlined by both Whitham [34] or Zauderer [35] that equations (19)–(22), (26)–(29) form a parabolic system of partial differential equations. This calculation is reported in detail for a nearly identical system by Caspar.

3. Thermal explosion theory

We develop a thermal explosion theory here which shows that when spatial homogeneity is assumed for most variables that three distinct periods can be identified. In the first and most physically relevant, the induction period, spatially homogeneous plastic work induces a temperature rise which brings the material to a temperature at which significant reaction ensues. This is in contrast to traditional thermal explosion theory, in which thermal explosion is caused by the accumulation of sufficient thermal energy due to slow reaction during the induction period. We give estimates for the induction time from (a) a plausible approximate theory which lacks full asymptotic rigour and (b) a more rigorous asymptotic theory found when the strain hardening parameter η takes on special values. The second period is the reaction period during which heat release due to chemical reaction primarily governs the process. In the third period, after reaction completion, plastic work again governs the process. It is noted that the model loses most of its physical validity soon after vigorous reaction commences. In particular, strong fluid phase effects become important, and the constitutive models for stress and reaction kinetics are beyond the domains in which they were calibrated. We nevertheless give predictions in all three periods in the interest of giving a full exposition of the strengths and weaknesses of models of this type.

A thermal explosion theory can be obtained in the following manner. We first make the assumption that $\hat{\epsilon}_T$ is negligibly small. Next it is assumed that temperature is a function of at most time, $T_* = T_*(t_*)$. A necessary, but not sufficient, condition for the second assumption is that $\widehat{Pe}$ be sufficiently large and temperature gradients sufficiently small to render thermal

diffusion negligible relative to plastic work and reaction. Then the following expressions satisfy equations (19), (22) and (23):

$$v_* = z_* \tag{30}$$

$$u_* = z_* t_*. \tag{31}$$

The specimen has a linear variation of circumferential velocity with axial distance. The solution describes a specimen subjected to a strain $\gamma_* = t_*$, which is spatially homogeneous and linearly increasing with time and a consequent strain rate, $\dot{\gamma}_* = 1$, which is constant. The average strain rate takes on the same value, $\overline{\dot{\gamma}}_* = 1$. By further assuming that the reaction progress variable is a function of time only, $\lambda_* = \lambda_*(t_*)$, equations (20) and (21) reduce to

$$\frac{\mathrm{d}T_*}{\mathrm{d}t_*} = \hat{\alpha}\widehat{Ec}\, T_*^{\nu} t_*^{\eta} + \hat{a}\hat{q}(1-\lambda_*)\exp\left(-\frac{\hat{\Theta}}{T_*}\right) \qquad T_*(0) = 1 \tag{32}$$

$$\frac{\mathrm{d}\lambda_*}{\mathrm{d}t_*} = \hat{a}(1-\lambda_*)\exp\left(-\frac{\hat{\Theta}}{T_*}\right) \qquad \lambda_*(0) = 0. \tag{33}$$

Equation (32) predicts that temperature changes in response to plastic work and chemical reaction; equation (33) predicts temperature-sensitive reaction to occur whenever there is unreacted material present. We can also form a supplementary equation for shear stress:

$$\tau_* = \hat{\alpha} T_*^{\nu} t_*^{\eta}. \tag{34}$$

3.1. Induction period

3.1.1. Approximate theory. The approximate thermal explosion theory is developed as follows. For cases in which temperature variation at early time is predominantly governed by the plastic work rate, temperature evolution is primarily governed by

$$\frac{\mathrm{d}T_*}{\mathrm{d}t_*} = \hat{\alpha}\widehat{Ec}\, T_*^{\nu} t_*^{\eta} \qquad t_* < t_{*i} \qquad T_*(0) = 1. \tag{35}$$

Here t_{*i} is defined as the induction time, before which chemical reaction does not significantly influence temperature. Equation (35) has the solution

$$T_*(t_*) = \left(\frac{1-\nu}{1+\eta}\hat{\alpha}\,\widehat{Ec}\, t_*^{\eta+1} + 1\right)^{1/(1-\nu)} \qquad t_* < t_{*i}. \tag{36}$$

An algebraic estimate for the induction time t_{*i} can be obtained by equating from equation (32) the plastic work rate term to the chemical reaction rate term, taking care to replace T_* by its estimate in the inert limit (36) and to consider λ_* to be negligibly small. These assumptions are verified later by a numerical analysis. The estimate is found from an appropriate root to the equation

$$\hat{\alpha}\widehat{Ec}\left(\frac{1-\nu}{1+\eta}\hat{\alpha}\widehat{Ec}\, t_{*i}^{\eta+1} + 1\right)^{\nu/(1-\nu)} t_{*i}^{\eta} = \hat{a}\hat{q}\exp\left[-\hat{\Theta}\left(\frac{1-\nu}{1+\eta}\hat{\alpha}\widehat{Ec}\, t_{*i}^{\eta+1} + 1\right)^{-1/(1-\nu)}\right]. \tag{37}$$

In general, equation (37) must be solved via a numerical technique. Temperature at $t_* = t_{*i}$ is defined to be T_{*i} and is found by evaluating equation (36) at the induction time t_{*i}. The special case where $\nu = -1$, $\eta = 1$ and $\hat{\alpha}\widehat{Ec}\, t_{*i}^2 \gg 1$, has the approximate explicit solution and dimensional counterpart

$$t_{*i} = \frac{\hat{\Theta}}{\sqrt{\hat{\alpha}\widehat{Ec}}\ln\left((\hat{a}\hat{q})/\sqrt{\hat{\alpha}\widehat{Ec}}\right)} \qquad t_i = \frac{LE}{\Re T_0 v_L\sqrt{\frac{\alpha}{\rho c T_0}}\ln\left(\frac{La}{v_L}\frac{\tilde{q}}{cT_0}/\sqrt{\frac{\alpha}{\rho c T_0}}\right)}. \tag{38}$$

In this limit, thermal explosion is hastened by increases in stress constant, Eckert number, kinetic rate constant, heat release and by decreases in activation energy.

3.1.2. Asymptotic theory. A similar asymptotic analysis can yield a complementary result in the limit of large activation energy, $\hat{\Theta} \gg 1$. In the induction zone we consider the following ordering of dependent variables:

$$T_* = 1 + \frac{1}{\hat{\Theta}} T_{*1} + \cdots \qquad \lambda_* = \frac{1}{\hat{\Theta}} \lambda_{*1} + \cdots \tag{39}$$

where $T_{*1} \sim \mathrm{O}(1)$ and $\lambda_{*1} \sim \mathrm{O}(1)$. Making these substitutions into equation (32) and retaining only O(1) quantities, we obtain a simpler differential equation for the temperature perturbation T_{*1}:

$$\frac{\mathrm{d}T_{*1}}{\mathrm{d}t_*} = \hat{\beta}_1 \left(t_*^{\eta} + \hat{\beta}_2 \mathrm{e}^{T_{*1}} \right) \qquad T_{*1}(0) = 0 \tag{40}$$

where the constants $\hat{\beta}_1$ and $\hat{\beta}_2$ are defined as

$$\hat{\beta}_1 = \hat{\Theta} \hat{\alpha} \widehat{Ec} \qquad \hat{\beta}_2 = \frac{\hat{a}\hat{q}}{\hat{\alpha} \widehat{Ec}\, \mathrm{e}^{\hat{\Theta}}}. \tag{41}$$

Rescaling time so that

$$\tilde{t}_* = \hat{\beta}_1^{1/(1+\eta)} t_* \tag{42}$$

allows transformation of equation (40) to

$$\frac{\mathrm{d}T_{*1}}{\mathrm{d}\tilde{t}_*} = \tilde{t}_*^{\eta} + \hat{\beta}_3 \mathrm{e}^{T_{*1}} \qquad T_{*1}(0) = 0 \tag{43}$$

where the constant $\hat{\beta}_3$ has the definition

$$\hat{\beta}_3 = \hat{\beta}_1^{\eta/(1+\eta)} \hat{\beta}_2. \tag{44}$$

In the high activation energy limit, the temperature dependence of the constitutive equation for stress is not important, nor is the effect of reactant depletion. We also see that plastic work effects dominate chemical reaction effects when $\hat{\beta}_3 \ll 1$.

We do not have a general solution for equation (43) but can find solutions in two special cases: $\eta = 0$, which implies there are no strain hardening effects, and $\eta = 1$, which implies a linear dependence of stress with strain. For $\eta = 0$, the solution is

$$T_{*1}(\tilde{t}_*) = \ln \left(\frac{\mathrm{e}^{\tilde{t}_*}}{1 + \hat{\beta}_3 \left(1 - \mathrm{e}^{\tilde{t}_*} \right)} \right). \tag{45}$$

Equation (45) predicts a monotonic increase in T_{*1} which reaches an infinite value at a finite time, which is the induction time $\tilde{t}_{*i0}$. This time is reached when the denominator of the argument of the logarithm is zero, giving $\tilde{t}_{*i0} = \ln((1 + \hat{\beta}_3)/\hat{\beta}_3)$. For $\hat{\beta}_3 \ll 1$, this reduces to $\tilde{t}_{*i0} = \ln(1/\hat{\beta}_3)$. In terms of the original scaling, the induction time is thus

$$t_{*i0} = \frac{1}{\hat{\beta}_1} \ln \frac{1}{\hat{\beta}_3} = \frac{1}{\hat{\Theta} \hat{\alpha} \widehat{Ec}} \ln \left(\frac{\hat{\alpha} \widehat{Ec} \mathrm{e}^{\hat{\Theta}}}{\hat{a}\hat{q}} \right) \qquad (\eta = 0). \tag{46}$$

When $\eta = 1$, equation (43) has a different closed form solution, namely,

$$T_{*1}(\tilde{t}_*) = \frac{1}{2} \tilde{t}_*^2 - \ln \left(1 - \hat{\beta}_3 \sqrt{\frac{\pi}{2}}\, \mathrm{erfi} \left(\frac{\tilde{t}_*}{\sqrt{2}} \right) \right) \tag{47}$$

where the imaginary error function,

$$\mathrm{erfi}(\xi) = \frac{1}{\mathrm{i}} \sqrt{\frac{2}{\pi}} \int_0^{\mathrm{i}\xi} \exp\left(-\zeta^2\right) \mathrm{d}\zeta \tag{48}$$

with ξ as an arbitrary variable and ζ as a dummy variable, has been employed. While the imaginary number i appears in its definition, it is noted that erfi maps real elements ξ into a strictly real range. Again, the solution for temperature perturbation, equation (47), becomes unbounded at finite induction time, which indicates the onset of thermal explosion. This occurs at $\tilde{t}_{*i1} = \sqrt{2}\,\mathrm{erfi}^{-1}(\sqrt{2/\pi}/\hat{\beta}_3)$. In terms of the original time scaling, this becomes

$$t_{*i1} = \sqrt{\frac{2}{\hat{\beta}_1}}\,\mathrm{erfi}^{-1}\left(\sqrt{\frac{2}{\pi}}\frac{1}{\hat{\beta}_3}\right) = \sqrt{\frac{2}{\hat{\Theta}\hat{\alpha}\widehat{Ec}}}\,\mathrm{erfi}^{-1}\left(\sqrt{\frac{2}{\pi}}\frac{\hat{\alpha}\widehat{Ec}\,\mathrm{e}^{\hat{\Theta}}}{\hat{a}\hat{q}}\right) \qquad (\eta = 1). \tag{49}$$

Away from the limits $\eta = 0$ and 1, one can integrate equation (43) numerically to determine the induction time predicted by the asymptotic theory.

3.2. Reaction period

We next estimate reaction time scales via local linear analysis. Assuming that chemical reaction dominates over plastic work in dictating temperature changes during the period of vigorous reaction, equations (32) and (33) are approximated for $t_* \geqslant t_{*i}$ as

$$\frac{\mathrm{d}T_*}{\mathrm{d}t_*} = \hat{a}\hat{q}(1-\lambda_*)\exp\left(-\frac{\hat{\Theta}}{T_*}\right) \qquad T_*(t_{*i}) = T_{*i} \tag{50}$$

$$\frac{\mathrm{d}\lambda_*}{\mathrm{d}t_*} = \hat{a}(1-\lambda_*)\exp\left(-\frac{\hat{\Theta}}{T_*}\right) \qquad \lambda_*(t_{*i}) = 0. \tag{51}$$

Subtracting the product of $\hat{q}$ and equation (51) from equation (50), an equation for energy conservation during vigorous reaction is obtained:

$$\frac{\mathrm{d}}{\mathrm{d}t_*}(T_* - \hat{q}\lambda_*) = 0. \tag{52}$$

Integrating and applying appropriate initial conditions yields

$$T_* - \hat{q}\lambda_* = T_{*i}. \tag{53}$$

Using equation (53) to eliminate T_* from equation (51), a single ordinary differential equation for λ_* is found during vigorous reaction:

$$\frac{\mathrm{d}\lambda_*}{\mathrm{d}t_*} = \hat{a}(1-\lambda_*)\exp\left(-\frac{\hat{\Theta}}{T_{*i} + \lambda_*\hat{q}}\right) \qquad \lambda_*(t_{*i}) = 0. \tag{54}$$

A linear analysis at the time of onset of vigorous reaction shows the reaction time constant just at ignition, t_{*iR}, has a value

$$t_{*iR} = \frac{1}{\hat{a}}\exp\left(\frac{\hat{\Theta}}{T_{*i}}\right). \tag{55}$$

A similar analysis near the point of complete reaction shows the time constant to have evolved to the faster

$$t_{*R} = \frac{1}{\hat{a}}\exp\left(\frac{\hat{\Theta}}{T_{*i} + \hat{q}}\right). \tag{56}$$

Thus, reaction evolves on scales which have an algebraic dependence on the kinetic constant and an exponential dependence on activation energy, temperature at ignition and heat release.

3.3. Post-reaction period

After completion of reaction, plastic work again dominates. Though at this point the constitutive model for stress is no longer in a regime which can be compared with experiment, the model predicts a return to a condition in which plastic work dictates the rate of temperature rise. Temperature can be predicted by solving equation (35) subject to the initial condition $T_*(t_{*i}) = T_{*i} + \hat{q}$, which has the solution

$$T_*(t_*) = \left(\frac{1-\nu}{1+\eta} \hat{\alpha} \widehat{Ec} \, (t_*^{\eta+1} - t_{*i}^{\eta+1}) + (T_{*i} + \hat{q})^{1-\nu} \right)^{1/(1-\nu)} \qquad t_* > t_{*i}. \tag{57}$$

4. Numerical methods

Here the numerical methods used to solve the governing equations are briefly described. In the next section, we solve the set of two ordinary differential equations which result from thermal explosion theory: equations (32) and (33). These equations are solved to a precision of 16 digits using the NDSolve routine in the Mathematica 3.0 software package. Solution time on a Sun UltraSparc 1 is under 1 min. Then, in the following section, a set of partial differential equations, equations (19)–(22), is solved for the spatially inhomogeneous problem. As the system is parabolic, the equations are suited to solution via a time-marching technique. The system is solved with a method-of-lines approach, embodied in a double-precision Fortran 77 computer code, on a uniform spatial grid of 49 nodes in a few minutes on the same machine. To implement the method of lines, spatial derivatives are represented as second-order spatially accurate centred finite differences. What results is a set of 196 (four equations for each of the 49 nodes) ordinary differential equations in time. These equations are solved implicitly using the method found in the standard LSODE subroutines [36]. While the implicit method does not have as severe restrictions on time step size as do explicit methods, an adaptive time-stepping procedure is employed to guarantee convergence of the Newton's method iteration required by the implicit method at each time step. The adaptive time step algorithm selects a time step so as to suppress large changes in any fundamental variables during any given time step. All solutions presented have a temporal accuracy appropriate for the level of spatial resolution employed. Reference [26] demonstrates convergence of error norms with grid size, consistent with the specified accuracy of spatial discretization.

5. Results

Here, results are presented first for the spatially homogeneous thermal explosion theory. Then a detailed comparison between the predictions of the spatially homogeneous and inhomogeneous theories, which highlights the generally small differences, is presented. Lastly, to demonstrate limits under which thermal explosion theory is a good predictor of ignition, the sensitivity of induction time to variation in initial temperature perturbation $\hat{\epsilon}_T$ is reported.

For all calculations we select a set of parameter values which models the explosive LX-14, chosen because of the ready availability of constitutive data. Dimensional and corresponding dimensionless values are listed in table 1, which are identical to those used in [27]. Thermochemical parameters are taken from Dobratz and Crawford [29], who describe this material by the chemical formula $C_{1.52}H_{2.92}N_{2.59}O_{2.66}$ and report that the material is 95.5% mass fraction granular HMX bound in a 4.5% estane (a co-polymer of polyester and polyurethane) binder. The mean particle size of the HMX grains is less than 250 μm. Mechanical properties were determined experimentally and the thermal softening exponent ν was estimated so that

Table 1. Parameters used in baseline numerical calculations [26, 27, 29].

Material properties		Reaction parameters		
α (N m^{-2})	4.239×10^7	a (s^{-1})	5.00×10^{19}	
ν	-1.28×10^0	$\tilde{q}$ (J kg^{-1})	5.95×10^6	
η	3.20×10^{-1}	E (J mol^{-1})	2.206×10^5	
μ	8.00×10^{-2}	$\Re$ (J mol^{-1} K^{-1})	8.314×10^0	
ρ (kg m^{-3})	1.849×10^3			
c (J kg^{-1} K^{-1})	1.130×10^3			
k (W m^{-1} K^{-1})	4.39×10^{-1}			
Test parameters		Dimensionless parameters		
v_L (m s^{-1})	7.00×10^0	$\hat{\alpha} = \dfrac{\alpha}{\rho v_L^2}$	4.68×10^2	
L (m)	2.50×10^{-3}	$\widehat{Ec} = \dfrac{v_L^2}{cT_0}$	1.46×10^{-4}	
T_0 (K)	2.98×10^2	$\widehat{Pe} = \dfrac{\rho c v_L L}{k}$	8.33×10^4	
			$\hat{a} = \dfrac{La}{v_L}$	1.79×10^{16}
			$\hat{q} = \dfrac{\tilde{q}}{cT_0}$	1.77×10^1
			$\hat{\Theta} = \dfrac{E}{\Re T_0}$	8.90×10^1
			$\hat{\beta}_3$	1.54×10^{-20}

the material lost significant strength near its melting point [26, 27]. The imposed strain rate was $\overline{\dot{\gamma}} = 2800$ s^{-1}.

5.1. Spatially homogeneous solutions

We solve equations (32) and (33) numerically. Figure 2 gives solutions for (*a*) $T_*(t_*)$, (*b*) $\lambda_*(t_*)$, (*c*) $\tau_*(t_*)$ and (*d*) the magnitude of the difference in temperature predictions between the numerical solution of equations (32) and (33) (labelled $T_{*\text{num}}$) and the approximate solutions of equations (36) and (57) (labelled $T_{*\text{app}}$) as a function of t_*. From figure 2(*a*) it is seen that the dimensionless temperature increases from its initial value of unity to a value of 2.18 (649 K) at the induction time of $t_{*i} = 15.13$ ($t_i = 5.40$ ms), predicted by iterative solution of equation (37). In fact, the crude explicit estimate of equation (38), $t_{*i} = 8.20$ ($t_i = 2.93$ ms), is only in error by a factor of roughly two. Additionally, numerical solution of the asymptotic temperature perturbation equation, equation (43), gives $t_{*i} = 5.77$ ($t_i = 2.07$ ms). Estimates are also found for special nearby values of η given by equation (46) ($t_{*i0} = 7.53$ ($t_{i0} = 2.69$ ms)) and by equation (49) ($t_{*i1} = 3.98$ ($t_{i0} = 1.42$ ms)). It is seen that for the parameters chosen, the less rigorous approximate theory somewhat better predicts the induction time than the asymptotic theory, most likely because the approximate theory retains the effect of a temperature-dependent stress and finite activation energy.

At the onset of vigorous reaction, the reaction is predicted to occur on time scales comparable to $t_{*iR} = 30.0$ ($t_{iR} = 10.7$ ms). However, near complete reaction, the model's exponential sensitivity of the reaction time scale to temperature induces evolution on scales of $t_{*R} = 5.1 \times 10^{-15}$ ($t_R = 1.8 \times 10^{-18}$ s). These very small scales are a direct consequence of using standard kinetic parameters for this material, albeit beyond the range in which the

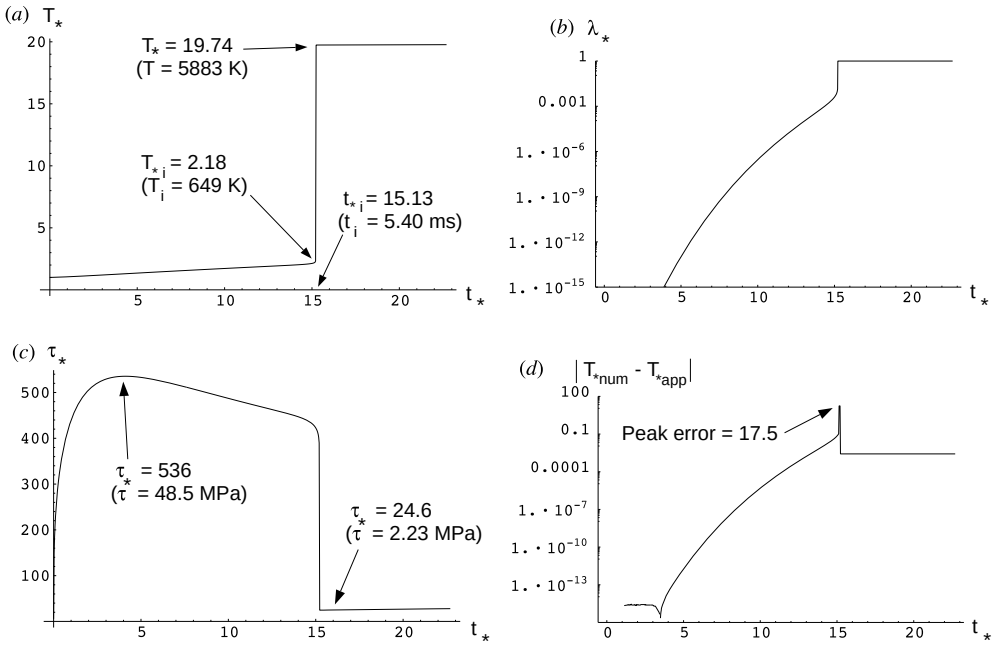

Figure 2. Temporal evolution of (*a*) temperature T_*, (*b*) reaction progress λ_*, (*c*) stress τ_* and (*d*) the magnitude of the difference of numerical predictions of temperature $T_{*\text{num}}$ from equations (32), (33) and predictions of the temperature approximations, $T_{*\text{app}}$: equations (36), (57) for simulations of LX-14, $\overline{\dot{\gamma}} = \dot{\gamma} = 2800\ \text{s}^{-1}$ using spatially homogeneous, thermal explosion theory.

parameters were experimentally calibrated. Near complete reaction, temperature is sufficiently high to have nearly overcome the model activation energy barrier and kinetics are being driven towards the limiting time constant given by the reciprocal of the kinetic prefactor: $1/\hat{a} = 5.6 \times 10^{-17}$ ($1/a = 2 \times 10^{-20}$ s). However, the kinetic prefactor and activation energy are typically estimated from a curve fit to experimental cook-off data far from the complete reaction limit, in which induction times may range from days to 10^{-4} s. A more physical model might explicitly account for both phonon interaction length and time scales and effects of porosity, crack growth and gas phase kinetics which must limit such high-temperature reactions. Even if such an accounting were made, it seems likely that reaction times would be extremely fine relative to induction times and the results would be indistinguishable when plotted simultaneously with induction time scale phenomena.

At complete reaction, temperature reaches a value of $T_* = 19.74$ ($T = 5883$ K). This high temperature is reasonable insofar as it is consistent with model assumptions and nearly identical to the sum, $T_* = 19.9$ ($T = 5914$ K), of the temperature at the induction time, $T_{*i} = 2.18$ ($T_i = 649$ K), and a simple estimate of the temperature rise which is attributable to reaction, $\hat{q} = 17.7$ ($\tilde{q}/c = 5265$ K). The small difference is attributed to the small amount of reaction which occurs in the induction period. Also, there is no mechanism in the thermal explosion model to reduce temperature. Additionally, it is shown in the next section that diffusion is too slow a mechanism to significantly reduce temperature during reaction. Further, the temperature after reaction would be reduced somewhat if account were taken of the increase in specific heat of the reaction products. After thermal explosion, the temperature resumes a relatively slow increase, which is difficult to perceive in figure 2(*a*), due to continued shearing.

The behaviour of λ_* is shown in figure 2(*b*) on a logarithmic scale. For $t_* < 4$, the extremely low values of λ_* are not plotted. For $0 < t_* < t_{*i}$, it is clear that there is a gradual increase in λ_*. When $T_* = T_{*i}$, the strong temperature sensitivity of the reaction rate induces a rapid change in λ_*, bringing it to unity over the same time scales as the temperature changes during the reaction.

In figure 2(*c*) the shear stress τ_* shows a rapid rise from zero to a peak of $\tau_* = 536$ ($\tau = 48.5$ MPa), realized at $t_* = 4.1$ ($t = 1.46$ ms), well before the induction time. At early time, strain and strain-rate hardening dominate over thermal softening. After the time of peak stress, thermal softening dominates. When $t_* = t_{*i}$, stress rapidly drops to $\tau_* \sim 24.6$ ($\tau \sim 2.23$ MPa), after which it slowly rises.

The plot of figure 2(*d*) demonstrates that the approximations to T_* are excellent for nearly all of the time domain. For $0 < t_* < 3.6$, the error is roughly 2×10^{-15}. In this domain, the difference between the numerical solution and the approximate solution is attributable to the error in the numerical solution of equations (32) and (33). While the Mathematica function NDSolve can solve to arbitrary precision, computation time increases with specified precision, so here precision is limited to 16 digit accuracy. Thus for $0 < t_* < 3.6$, equation (36) gives the more accurate prediction. For $t_* \geqslant 3.6$, the difference can be attributed to errors in the approximate solution. For $t_* < t_{*i}$, the approximate solution neglects influences of the reaction; this is manifested in a gradual increase in the difference up to the time of thermal explosion seen in the period $3.6 \leqslant t_* < 15.13$. The difference, however, is large just around the time of thermal explosion and has a magnitude of $|T_{*\mathrm{num}} - T_{*\mathrm{app}}| = 17.5$. In this region, with no explicit closed-form solution with structure available, the solution is approximated as a Heaviside step function. The consequent error is evident for an extremely short duration. After thermal explosion, equation (57) predicts temperature very well, as the difference is seen to drop roughly to the value of error accumulated during build-up to thermal explosion, near $|T_{*\mathrm{num}} - T_{*\mathrm{app}}| = 0.002$. The fact that the differences are of widely varying order of magnitude is a reflection of the absence of a formal asymptotic formulation of the approximate equations. Nevertheless, it is clear that the approximate formula performs well in predicting the temperature.

5.2. Spatially inhomogeneous solutions

To verify the ability of spatially homogeneous theory to accurately predict induction times as compared to the more robust spatially inhomogeneous theory, solutions from the previous section are compared to solutions of equations (19)–(23). In these calculations, temperature perturbation parameters are held fixed at $\hat{\epsilon}_T = 0.0116$, $\hat{\epsilon}_L = 0.02$. The dimensional value of temperature perturbation is 3.5 K and the dimensional zone width is 50 μm. All other parameter values are as given in table 1. Calculation was ceased after complete reaction was achieved in the centremost cell, at which time the computational time step was of the order of $\Delta t_* \sim 1 \times 10^{-16}$ ($\Delta t \sim 4 \times 10^{-20}$ s).

Once again these extremely small time scales are a consequence of the model assumptions. The kinetic model has not been calibrated for such fine time scales and in actuality neglected molecular level physical mechanisms which are most likely to be limiting the reaction rate in this period. While early portions of the calculation can be computed rapidly, the computation is extremely sluggish upon commencement of reactive shear banding, due to stiffness from chemical reaction and shear localization. As the key feature is the onset of ignition, and the constitutive model becomes less valid as more reaction products are present, it is reasonable to report results only up to ignition. It is noted that adaptive methods, such as the adaptive Chebyshev pseudo-spectral method recently employed by Bayliss *et al* [37] on

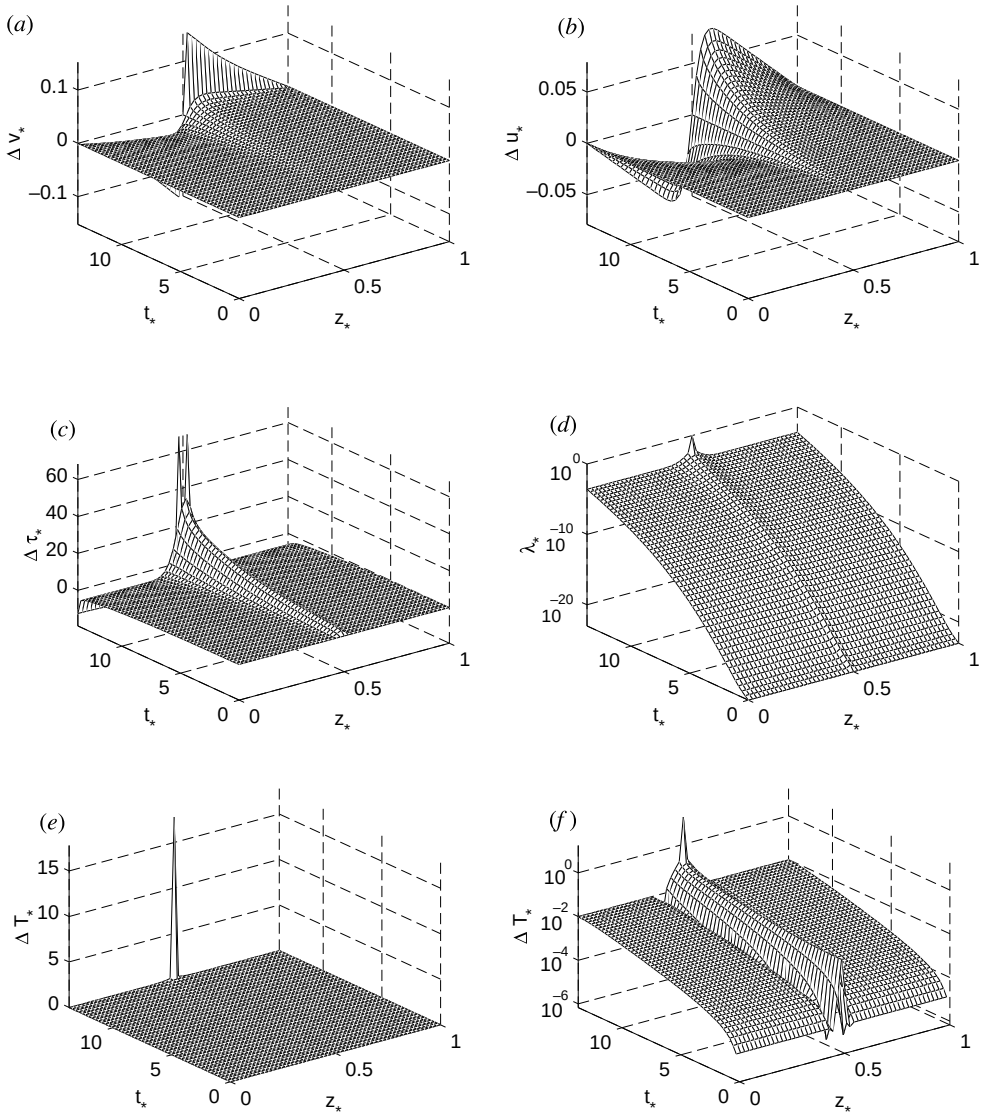

Figure 3. Time and space variation of difference (Δ) between predictions of spatially inhomogeneous theory and thermal explosion theory for (*a*) velocity Δv_*; (*b*) displacement Δu_*; (*c*) stress, $\Delta\tau_*$; (*d*) reaction progress, λ_* (note, not a difference); (*e*) temperature ΔT_* (absolute scale) and (*f*) temperature ΔT_* (logarithmic scale), for LX-14, $\dot{\bar{\gamma}} = 2800\ \text{s}^{-1}$.

an inert shear banding problem, could likely be used effectively to overcome the stiffness near localization.

Predictions are shown in figure 3. Except for figure 3(*d*), all plots in this figure represent the difference (Δ) between predictions of spatially inhomogeneous theory and thermal explosion theory. As can be seen differences are near zero for $t_* \ll t_{*i} \sim 13.73$ ($t_i \sim 4.90$ ms), both spatially inhomogeneous and thermal explosion theories give nearly identical results during the induction period. Near $t_* = t_{*i}$, shear begins to localize near the site of the initial

small inhomogeneity at $z_* = \frac{1}{2}$ ($z = 1.25$ mm) and differences become more pronounced. Nevertheless, it is noted that the magnitude of differences is quite small for the bulk of the induction period; the scaling employed in figure 3 highlights those differences that do exist.

Figure 3(*a*) gives the difference of velocity predictions of the full model and that of equation (30). The differences are near zero at early time and approach a peak of $\Delta v_* = 0.15$ ($\Delta v_\theta = 1.05$ m s^{-1}) at the cessation of calculation, at which time the strain rate at the centre of the shear band, calculated by a finite difference centred over two cells, is predicted to be $\dot{\gamma}_* = 7.5$ ($\dot{\gamma} \sim 2 \times 10^4$ s^{-1}). This should be considered a lower bound dictated by the finite spatial resolution employed, as it is noted that it is of the same order of magnitude as the finite difference assuming a full drop of velocity over two cells: $1/2\Delta z_* = 25$ ($v_L/2\Delta z = 7 \times 10^4$ s^{-1}).

Figure 3(*b*) gives differences in displacement, Δu_*, which reach a peak of $\Delta u_* = 0.079$ ($\Delta u_\theta = 0.20$ mm) at cessation of calculation. Thermal explosion theory values for displacement are given by equation (31). Stress differences, with thermal explosion values from equation (34), are shown in figure 3(*c*), which are near zero for most of the domain and reach a peak of $\Delta\tau_* = 68.4$ ($\Delta\tau = 6.2$ MPa) at cessation of calculation. As we have no analytic estimate for λ_* in the induction period, figure 3(*d*) plots the magnitude of λ_* for the full calculation on a logarithmic scale. The nearly spatially uniform rise is evident, with a small, but important, tendency for reaction to predominate in the vicinity of the temperature perturbation. It is seen that the centremost cell has progressed to complete reaction, $\lambda_* = 1$, at cessation of calculation.

Figures 3(*e*) and (*f*) give plots of the difference in temperature predictions of the full model and those of equation (36), on an absolute and logarithmic scale, respectively. The absolute scale prediction highlights the accuracy of the approximate solution for the bulk of the domain, except at the ignition point, where the difference is $\Delta T_* = 17.8$ ($\Delta T = 5304$ K). The large difference exists because the two theories predict slightly different times for thermal explosion. The inhomogeneous theory predicts an absolute peak temperature of $T_* = 19.77$ ($T = 5892$ K), almost identical to that predicted by thermal explosion theory: $T_* = 19.74$ ($T = 5883$ K). One might expect that diffusion would lower the peak predicted by the inhomogeneous theory. However, it is recalled from classical thermal diffusion theory that the time necessary for diffusion to play a significant role in reducing temperature over one finite-difference cell size is $t_{*D} = \widehat{Pe}\Delta z_*^2$, which, for this problem, is $t_{*D} = 33.3$ (11.9 ms), orders of magnitude greater than the reaction time scale, and about twice as long as the induction time scale. Hence it is not surprising that even when diffusion is included, that high localized temperatures are predicted; moreover, the differences are likely to be due to numerical truncation errors. The plot on the logarithmic scale highlights the evolution of the temperature perturbation and the slow accumulation of error due to neglect of reaction in the approximation of equation (36).

The induction time, defined here as the time at which $\lambda_* = \frac{1}{2}$ in the centremost cell, is $t_{*i} = 13.73$ ($t_i = 4.90$ ms), about 10% less than that predicted by thermal explosion theory. The difference is dependent on the magnitude of the initial temperature perturbation, as shown in figure 4. A perturbation of $\hat{\epsilon}_T = 0$ gives identical results to thermal explosion theory. As the perturbation increases, the induction time slowly decreases, until the perturbation becomes of a similar order of magnitude as the activation energy $\hat{\Theta}$. Then, the induction time drops rapidly with increasing $\hat{\epsilon}_T$ until it reaches a limiting value dictated by the reciprocal of the kinetic prefactor: $1/\hat{a}$. It is noted that large values of $\hat{\epsilon}_T$ correspond to generally unrealizable temperatures; they are included to show the global mathematical character of the response.

A preferable limiting study would model temperature perturbation as a Dirac delta function, whose strength gave a measure of the energy of the perturbation. One would then

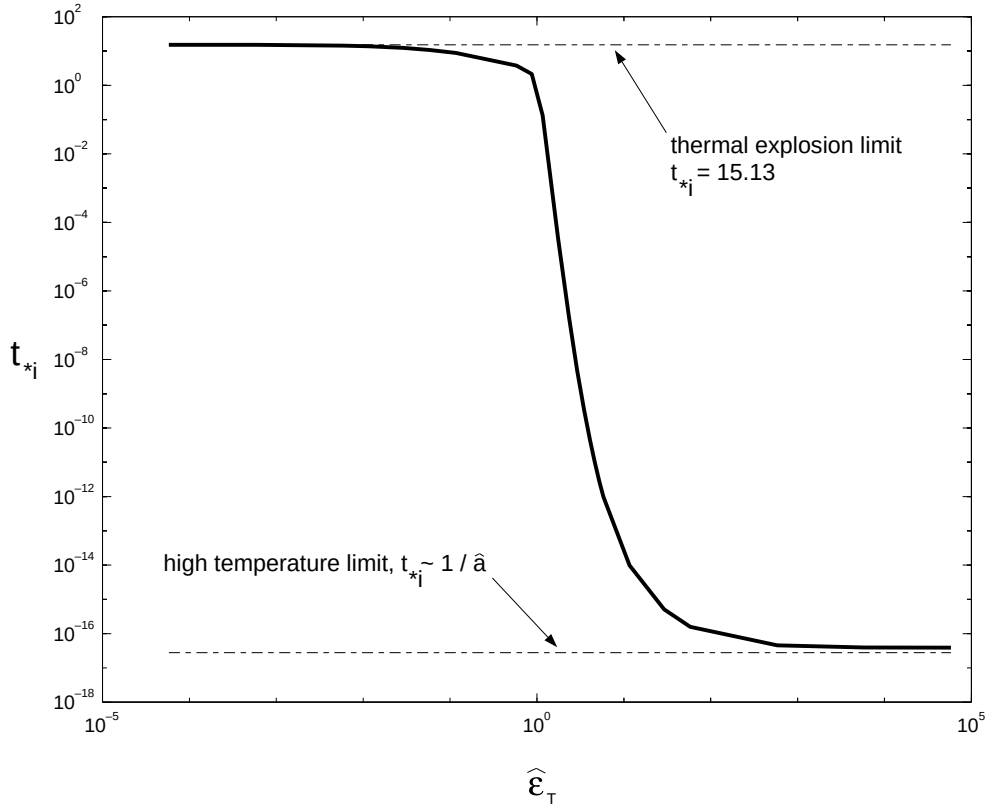

Figure 4. Variation of induction time, t_{*i}, with the magnitude of the initial temperature perturbation, $\hat{\epsilon}_T$.

study ignition sensitivity as the energy perturbation was varied. However, proper consideration of this problem would require extremely fine grids. A finite-difference model of this would deposit all energy in one very thin cell. The temperature would be high enough to induce a high-order reaction which would evolve on a time scale of $t_{*R} = 1/\hat{a}$. The reaction would face competition from thermal diffusion. To model this properly, the thermal diffusion time for a cell of width Δz_* would need to be at least as small as the reaction time. With the thermal diffusion time as $t_{*D} = \widehat{Pe}\Delta z_*^2$, the resulting spatial discretization limit is $\Delta z_* < \sqrt{1/(\hat{a}\widehat{Pe})}$. For the parameters of table 1, this would require $\Delta z_* < 2.6 \times 10^{-11}$ (6.5×10^{-14} m) which, in addition to giving rise to difficulties with the continuum assumption, would be difficult to model given present computational limitations.

6. Conclusions

It is evident from the results for the HMX-based material LX-14 that a spatially homogeneous thermal explosion model for a strained energetic solid is adequate to predict ignition, even in the presence of small perturbations which can induce shear localization. Indeed, enhanced plastic work during a localization event will accelerate reaction in the region of localization; however, at this time the surrounding material is also at the threshold of reaction. As thermal

diffusion is seen to be a relatively slow event, it is predicted that the material surrounding a vigorously reacting shear-localized hot spot will not react as a consequence of diffusion of energy from the hot spot, but rather will react because of the accumulated thermal energy during the relatively long period of homogeneous plastic work. That is, relatively large hot spots associated with regions of homogeneous shear and significant material strength induce reaction; more concentrated reactive hot spots associated with possible shear localization are simply harbingers of an already imminent ignition process, and not its cause. Similar conclusions may be valid for any material which reacts at a temperature near the temperature where material strength is lost, such as HMX, but could potentially be quite different for classes of energetic material without this property.

Acknowledgments

The unsteady code used is the author's modification of a code written by Mr R J Caspar. The work was supported by AFOSR through the Summer Research Extension Program under contract RDL-96-0870.

References

[1] Bowden F P and Yoffe Y D 1952 *Initiation and Growth of Explosion in Liquids and Solids* (Cambridge: Cambridge University Press)

[2] Field J E, Swallowe G M and Heavens S N 1982 Ignition mechanisms of explosives during mechanical deformation *Proc. R. Soc.* A **382** 231–44

[3] Bai Y and Dodd B 1992 *Adiabatic Shear Localization: Occurrence, Theories, and Applications* (New York: Pergamon)

[4] Dilellio J A and Olmstead W E 1997 Shear-band formation due to a thermal flux inhomogeneity *SIAM J. Appl. Math.* **57** 959–71

[5] Howe P M, Gibbons G and Webber P 1985 An experimental investigation of the role of shear in initiation of detonation by impact *8th Int. Symp. on Detonation* (Annapolis, MD: Naval Surface Weapons Center) pp 294–301

[6] Mohan V K, Bhasu V C J and Field J E 1989 Role of adiabatic shear bands in initiation of explosives by drop-weight impact *9th Int. Symp. on Detonation* (Arlington, VA: Office of Naval Research) pp 1276–83

[7] Chen H C, Nesterenko V F, Lasalvia J C and Meyers M A 1997 Shear-induced exothermic chemical-reactions *J. Physique IV* **7** 27–32

[8] Boyle V, Frey R and Blake O 1989 Combined pressure shear ignition of explosives *9th Int. Symp. on Detonation* (Arlington, VA: Office of Naval Research) pp 3–17

[9] Coffey C S, Frankel M J, Liddiard T P and Jacobs S J 1981 Experimental investigation of hot spots produced by high rate deformation and shocks *7th Int. Symp. on Detonation* (Annapolis, MD: Naval Surface Weapons Center) pp 970–5

[10] Coffey C S 1989 Initiation of explosive crystals by shock or impact *9th Int. Symp. on Detonation* (Arlington, VA: Office of Naval Research) pp 58–65

[11] Coffey C S 1991 The localization of energy and plastic-deformation in crystalline solids during shock or impact *J. Appl. Phys.* **70** 4248–54

[12] Field J E, Palmer S J P, Pope P H, Sundararajan R and Swallowe G M 1985 Mechanical properties of PBX's and their behaviour during drop weight impact *8th Int. Symp. on Detonation* (Annapolis, MD: Naval Surface Weapons Center) pp 635–44

[13] Kipp M E 1985 Modeling granular explosive detonations with shear band concepts *8th Int. Symp. on Detonation* (Annapolis, MD: Naval Surface Weapons Center) pp 35–41

[14] Swallowe G M and Field J E 1981 Effect of polymers on the drop-weight sensitiveness of explosives *7th Int. Symp. on Detonation* (Annapolis, MD: Naval Surface Weapons Center) pp 24–35

[15] Winter R E and Field J E 1975 Role of localized plastic-flow in impact initiation of explosives *Proc. R. Soc.* A **343** 399

[16] Field J E, Bourne N K, Palmer S J P, Walley S M and Smallwood J M 1992 Hot-spot ignition mechanisms for explosives and propellants *Phil. Trans. R. Soc.* A **339** 269–83

[17] Bonnett D L and Butler P B 1996 Hot-spot ignition of condensed-phase energetic materials *J. Propulsion Power* **12** 680–90
[18] Ho S Y 1992 Impact ignition mechanisms of rocket propellants *Combust. Flame* **91** 131
[19] Ho S Y 1996 High strain-rate impact studies of predamaged rocket propellants. I. characterization of damage using a cumulative damage failure criterion *Combust. Flame* **104** 524–34
[20] So W and Francis E C 1991 Dynamic finite-element analysis of solid-propellant impact test *J. Spacecraft Rockets* **28** 658–62
[21] Chaudhri M M 1989 The initiation of fast decomposition in solid explosives by fracture, plastic flow, friction, and collapsing voids *9th Int. Symp. on Detonation* (Arlington, VA: Office of Naval Research) pp 857–67
[22] Chaudhri M M 1976 Slab initiation of explosions *Nature* **263** 121–2
[23] Dodd B and Atkins A G 1983 Flow localization in shear deformation of void-containing and void-free solids *Acta Metal.* **31** 9–15
[24] Frey R B 1981 The initiation of explosive charges by rapid shear *7th Int. Symp. on Detonation* (Annapolis, MD: Naval Surface Weapons Center) pp 36–42
[25] Dienes J K 1986 On reactive shear bands *Phys. Lett.* A **118** 433–8
[26] Caspar R J 1996 Experimental and numerical study of shear localization as an initiation mechanism in energetic solids *MS Thesis* University of Notre Dame
[27] Caspar R J, Powers J M and Mason J J 1998 Investigation of reactive shear localization in energetic solids *Combust. Sci. Technol.* **136** 349–71
[28] Davidson J E and Beckstead M W 1997 Improvements to steady-state combustion modeling of cyclotrimethylenetrinitramine *J. Propulsion Power* **13** 375–83
[29] Dobratz B M and Crawford P C 1985 *LLNL Explosives Handbook—Properties of Chemical Explosives and Explosive Simulants* Lawrence Livermore National Labs UCRL-52997 National Technical Information Service DE91–006884
[30] Baer M R and Nunziato J W 1986 A two-phase mixture theory for the deflagration-to-detonation transition (DDT) in reactive granular materials *Int. J. Multiphase Flow* **12** 861–89
[31] Gonthier K A and Powers J M 1996 A numerical investigation of transient detonation in granulated material *Shock Waves* **6** 183–95
[32] DiLellio J A and Olmstead W E 1997 Temporal evolution of shear band thickness *J. Mech. Phys. Solids* **45** 345–59
[33] Clifton R J, Duffy J, Hartley K A and Shawki T G 1984 On critical conditions for shear band formation at high strain rates *Scr. Metall.* **18** 443–8
[34] Whitham G B 1974 *Linear and Nonlinear Waves* (New York: Wiley)
[35] Zauderer E 1983 *Partial Differential Equations of Applied Mathematics* (New York: Wiley)
[36] Hindmarsh A C 1983 ODEPACK, A systematized collection of ODE solvers *Scientific Computing* ed R S Stepleman *et al* (Amsterdam: IMACS/North-Holland) pp 55–64
[37] Bayliss A, Belytschko T, Kulkarni M and Lott-Crumpler D A 1994 On the dynamics and the role of imperfections for localization in thermo-viscoplastic materials *Modelling Simul. Sci. Engng* **2** 941–64